Journal of Energy Storage 85 (2024) 111032

Contents lists available at ScienceDirect

Journal of Energy Storage

journal homepage: www.elsevier.com/locate/est

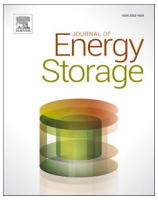

Research papers

Polyvinylidene fluoride supported phase change material fibers fabricated via emulsion jet injection method

Mikel Duran [a,b,*], Angel Serrano [a], Artem Nikulin [a], Jean-Luc Dauvergne [a], Jalel Labidi [b], Elena Palomo del Barrio [a,c]

[a] Centre for Cooperative Research on Alternative Energies (CIC energiGUNE), Basque Research and Technology Alliance (BRTA), Alava Technology Park, Albert Einstein 48, 01510 Vitoria-Gasteiz, Spain
[b] University of the Basque Country (UPV/EHU), Plaza Europa, 1, 20018 Donostia-San Sebastián, Gipuzkoa, Spain
[c] Ikerbasque, Basque Foundation for Science, 48013 Bilbao, Spain

ARTICLE INFO

Keywords:
Phase change material
Fiber
Microfluidics
Solvent extraction
PVDF
Thermal management

ABSTRACT

The manufacture of fibers with thermoregulatory properties is generating increasing interest, given the ease with which these materials can be adapted to different geometries and applications such as the production of thermoregulating textiles, flexible sensors and human health care. In this sense, the encapsulation of phase change materials (PCMs) into microfibers is a promising option, given the high amount of energy that these materials can store/release at almost constant temperature. The predominant methods to produce microfibers with encapsulated PCMs lack a compromise between simplicity and final enthalpy, needing to use complex methods to obtain fibers with high PCM content. In this sense, this work presents a method that meets both simplicity and final enthalpy to produce polyvinylidene fluoride (PVDF) fibers with encapsulated PCMs. To achieve this, the emulsion jet injection method has been combined with the use of the polymer itself as an emulsion stabilizer, avoiding using surfactants. With this method fibers with up to 137 J/g of latent heat, which is the highest value obtained for polymeric fibers with encapsulated PCMs produced by microfluidic approaches, and a PCM content of 63 % have been produced. This has been favored by the polymer content in the precursors which, as shown by SEM and droplet size measurements, favors the stability of the emulsions, stabilizing the system during fiber production and increasing the final PCM content. Finally, thermal cycling tests of the fibers have shown a complete PCM retention capacity in DSC and 64 % of its enthalpy after being submitted to 1500 cycles sequentially in both air and water environments.

1. Introduction

Flexible phase change materials (PCMs) are an emerging class of thermoregulatory materials that offer substantial potential in a wide range of smart applications, such as thermal management of electronic devices, human health care and comfort, thermal energy storage, photovoltaic systems, building materials and electrical vehicle battery cooling systems among others [1–4]. Apart from their ability to store/release thermal energy at near-constant temperature, these materials can withstand some deformation and, therefore, adapt to objects with complex geometries while ensuring good thermal contact. To realize the flexibility several methods have been proposed: {1} confinement of PCM into flexible porous scaffolds, {2} encapsulation of PCM into elastic shells, and {3} development of intrinsically flexible PCM based on molecularly engineered structures [5]. Considering device-level flexibility, the encapsulation of PCMs into polymeric microfibers have been growing interest. Indeed, microfibers can be used directly to create thermoregulated layers around complex objects [6], to produce films and fabrics that can then be incorporated into objects with flat or curved geometries [7], and to fabricate smart textiles with advanced thermoregulatory properties that can be applied for personal thermal management and protection [8,9].

Different strategies can be followed to produce polymeric fibers with encapsulated PCMs. In most of the cases found in bibliography, prefabricated microencapsulated PCMs (mainly core & shell microcapsules) are added to polymeric solutions to produce fibers by melt or solution

* Corresponding author at: Centre for Cooperative Research on Alternative Energies (CIC energiGUNE), Basque Research and Technology Alliance (BRTA), Alava Technology Park, Albert Einstein 48, 01510 Vitoria-Gasteiz, Spain.
E-mail address: mduran@cicenergigune.com (M. Duran).

https://doi.org/10.1016/j.est.2024.111032
Received 20 September 2023; Received in revised form 16 February 2024; Accepted 17 February 2024
Available online 26 February 2024

spinning. This allows to produce composite polymer-PCM fibers in a simple way, but the obtained PCM contents and enthalpy values of the final fibers are relatively low, not overpassing 40 J/g [10–12].

Another strategy is the filling of prefabricated polymeric fibers with PCMs in liquid state. In this case, hollow or porous polymeric fibers are produced (e.g., melt spinning, solvent extraction…) and then filled by injection, vacuum infiltration, or impregnation [13–16]. In this case, the obtained PCM contents increase noteworthily, and the obtained enthalpy values range between 70 and 180 J/g. Nevertheless, these strategies sacrifice simplicity for the increase of PCM content, as they require multiple steps.

Electrospinning techniques have also been used for PCMs encapsulation into polymeric fibers. They are based on coaxial jet (co-electrospinning [17–20] or emulsion jet (emulsion-electrospinning [21,22] elongation under electric field. Compared to the methods described above, electrospinning allows achieving similar enthalpy values in the final products (70–130 J/g) in one-single step instead of using multi-step process. However, electrospinning also presents some drawbacks such as low production rate and the use of high voltage sources. Moreover, electrospinning directly produces a matt of nanofibers instead of single fibers, thus reducing versatility and diversity of applications.

On the other side, microfluidics is widely used for the encapsulation of a wide range of materials into microcapsules due to the high control that provides on parameters such as capsule size and core content among others. Nevertheless, it requires the precise control of several fluid flow rates for the formation of single and double emulsions [23]. For this reason, microfluidic is still an emerging method in the encapsulation of phase change materials where the microfluidic devices for this purpose are mostly handmade, giving place to few examples of core & shell PCM/Polymer microcapsules successfully produced [24–28]. To the best of our knowledge, PCM encapsulation into polymeric fibers by microfluidic approaches has only been explored in few works [6,29] apart from our prior work published in 2023 [30]. The proposed method is based on gravity-aided emulsion jet injection into a bulk fluid, where fibers are produced by a solvent extraction mechanism governed by a Nonsolvent Induced Phase Separation (NIPS). This way PCP/PVDF fibers with up to 98 J/g of latent heat were produced without the need of multistep processes or high-voltage sources. Moreover, the method is surfactant-free, and the produced fibers withstand up to 1000 melt/crystallization cycles showing a mass loss of only 3.5 wt%. However, despite the advantages of the method in terms of simplicity, its competitiveness with respect to the above-mentioned strategies could be questionable due to the enthalpy values achieved in the fibers. These low values of latent heat result from a non-uniform PCM distribution and instability of injected emulsion that favor PCM losses during the solvent extraction process. Therefore, to date, the methods to produce fibers containing PCMs are either very complex; requiring multiple steps, increasing costs, and limiting their scalability; or are not able to produce fibers with high PCM contents.

Considering this, **the primary objective of the present work** is to place emulsion jet injection strategy as a and competitive alternative for the methods used to produce polymeric fibers with encapsulated PCMs, allowing to obtain higher enthalpy of the fibers in a simpler way. Therefore, this study aims to significantly improve our previous results; that is, increasing the amount of PCM that is encapsulated in the fibers and, therefore, their latent heat, without sacrificing the simplicity of the method and the use of surfactant-free emulsions. To this end, the PVDF used as raw material for the fibers will be used as emulsion stabilizer by increasing its concentration in the precursors. The effect of PVDF content in the precursor emulsion on the morphology, crystalline structure, and mechanical properties of pure PVDF fibers was analyzed. On the other side, the effect of the polymer concentration on the droplet size of the precursor emulsions, as well as in the final encapsulation of the PCMs and their distribution was also studied.

On the other hand, the way in which fibers are usually assessed in bibliography for their use under working conditions could be considered as low stringency, since most of the cycling tests performed are usually under inert or isothermal conditions. For this reason, **the secondary objective of this work** is to evaluate in a deeper way the reliability of the fibers under more realistic working conditions. To that end, a novel cycling test of 1000 cycles in air atmosphere and 500 cycles in water immersion was carried out. During this test mass losses, enthalpy changes and PCM content changes were analyzed to obtain information about the PCM retention capacity and aging of the fibers that nowadays is difficult to find in bibliography.

2. Experimental section

2.1. Materials

Commercial PVDF Solef® 5130 from SOLVAY was dissolved in *N*,*N*-Dimethylformamide (DMF) (99.5\% Pure) from EMPARTA®. This solution was used as a precursor for fiber production. Paraffin RT-25HC with a melting point between 22 and 26 °C and latent heat of 230 J/g was supplied by Rubitherm® and used as core material of the composite fibers. All chemicals were used as received with no further purification. Tap water was utilized for the DMF extraction process.

2.2. Precursor solution preparation

Two kinds of precursor solutions were prepared to produce pure PVDF and composite fibers. The materials and quantities used for their preparation are summarized in Table 1. The precursor for the pure PVDF fibers consisted of a 5 %, 7.5 % and 10 % by mass solution of PVDF in DMF that were prepared by dissolving PVDF in DMF at 60 °C with continuous stirring. As a precursor of the composite fibers, the same PVDF solutions were mixed withRT-25HC to obtain a 1:1 PVDF:RT-25HC weight proportion. These mixtures were emulsified by sonication in an ultrasound bath (S60H Elmasonic) at 40 °C for 30 min. No surfactant was used to stabilize the emulsion.

2.3. Fiber production

The experimental protocol followed from the initial precursor preparation to the final manufacture of the fibers is summarized in Fig. 1. The fibers were produced by injection of the precursor solutions into tap water in the same setup used for our previous work [30]. The precursors were injected through a capillary glass into a glass beaker filled with tap water. When the precursors get in contact with water, a liquid-liquid solvent extraction process took place, extracting DMF from the precursors and giving place to the solidification of PVDF into the shape of fibers. The fast solidification process trapped the RT-25HC emulsion inside the fiber structures, giving place to its encapsulation. A syringe pump (Pump 11 – Pico Plus Elite from HA Harvard Apparatus) was used to support the flow of precursor from the syringe to the glass capillary, that were connected by a PTFE tube. In this study the injection flowrate was readjusted with respect to our previous work, fixing it to 0.2 mL/min to promote the stability of the precursor jet during the fiber production. The glass beaker and the air surrounding the experimental setup were heated up to 30 °C by an electric fan-heater to ensure homogeneous temperature of the setup. After the injection process, the

Table 1
Material amounts used for the different precursors.

Sample	DMF (g)	PVDF (g)	RT-25HC (g)
PVDF-5	28.50	1.50	0
PVDF-7.5	27.75	2.25	0
PVDF-10	27.00	3.00	0
$PVDF_{PCM}$-5	28.50	1.50	1.50
$PVDF_{PCM}$-7.5	27.75	2.25	2.25
$PVDF_{PCM}$-10	27.00	3.00	3.00

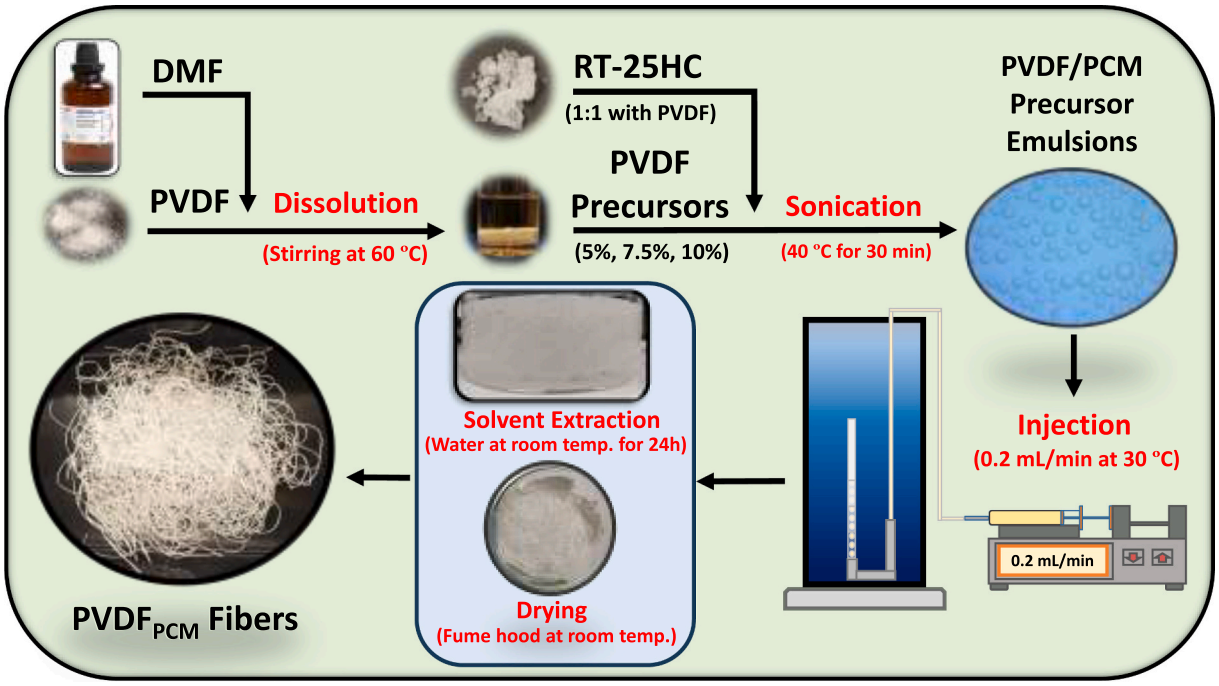

Fig. 1. Summarized squeme of the fiber manufacture protocoll.

fibers were collected and stored in tap water (room temperature) for 24 h to maximise DMF extraction and then were dried at room temperature in a fumehood.

2.4. Characterization

2.4.1. Scanning electron microscopy

To analyse the microstructure of the fibers, samples were imaged by means of a scanning electron microscope Quanta 200 FEG operated in low vacuum mode at 10 kV featured with a backscattered electron detector (BSED). Samples for morphological analysis were prepared as follows: for cross-section image acquisition, fibers were broken with the help of tweezers under liquid nitrogen for preserving their original shape and avoiding fiber flattening; the longitudinal section images were obtained by cutting the samples with a scalpel.

2.4.2. DSC analysis

DSC was used to determine the temperatures of phase transition and their corresponding latent heats. A power-compensation DSC Q2500 from TA Instruments was employed with sealed aluminium crucibles. The mass of the samples was ca. 9 mg. Argon (50 mL/min) was employed as purge gas. Each sample was subjected to three cycles of heating and cooling, with a heating/cooling rate of 5 °C/min. The transition temperatures were determined by the onset temperature of the corresponding endothermic peaks in the DSC-thermograms, whereas the latent heat was calculated by integration of the latter assuming a linear baseline. The DSC was calibrated for heat flow and temperature using high purity (>99.99\%) reference materials indium and sapphire. The accuracy in the determination of melting temperatures is ±0.5 °C, whereas that for the enthalpy of phase transition and specific heat is ±5\ %.

2.4.3. Thermal stability

Thermogravimetric analysis of the fibers and raw materials was performed in a TG209F1 Libra® Thermogravimetric Analyzer from NETZSCH. The analysis was based on a heating ramp from room temperature to 600 °C with a heating rate of 10 °C/min under nitrogen atmosphere.

2.4.4. Crystallinity measurements

The crystallinity of the raw PVDF powder and the produced fibers was determined by comparing their latent heat of melting (ΔH_m) to 104.7 J/g, which is the corresponding latent heat of fusion for pure PVDF crystals [31]. The needed melting point and enthalpy values were measured by DSC, the samples were heated from room temperature to 200 °C at a heating rate of 5 °C/min to ensure the complete melting of the materials.

2.4.5. Crystalline phase identification (FT-IR)

The crystalline phases of the PVDF fibers were identified by Fourier transform infrared (FT-IR) measurements performed in an infrared spectrophotometer Bruker Vertex 70v in the range of 4000 to 400 cm^{-1} with a resolution of 1 cm^{-1}.

2.4.6. Droplet size measurement

The droplet sizes of the different precursor emulsions were visualized and captured with an optical microscope ZEISS AXIO SCOPE.A1. From these pictures the droplet size distribution was calculated for each emulsion by using the software ImageJ 2.0 [32]. At least 200 droplet diameters were collected for each emulsion.

2.4.7. Cyclability and leakage test

A leakage test was carried out in the same setup used in our previous work [30] to check both cyclability and the PCM retention capacity of the fibers. The setup and the different sample configurations can be seen in Fig. 2. A fiber sample (200 mg) was placed onto a Peltier element, covered with absorbing paper, and then pressed with an aluminium block of 61 g (40x40x13 mm) to ensure a homogeneous temperature distribution and good contact between the fiber and the absorbing paper. The pressure exerted by the block would intensify any PCM leakage, so the conditions of this test can be considered as adverse. 1000 thermal cycles were performed from 10 to 40 °C. Isotherms of 120 s were held at maximum and minimum temperatures for each cycle.

For the cycling test in water, the same fiber sample was introduced in a “zip” plastic bag (60 × 80 mm) and filled up with water (10 mL). This bag was placed on the Peltier element, covered with thermal insulation, and pressed with the same aluminium block. 500 thermal cycles were

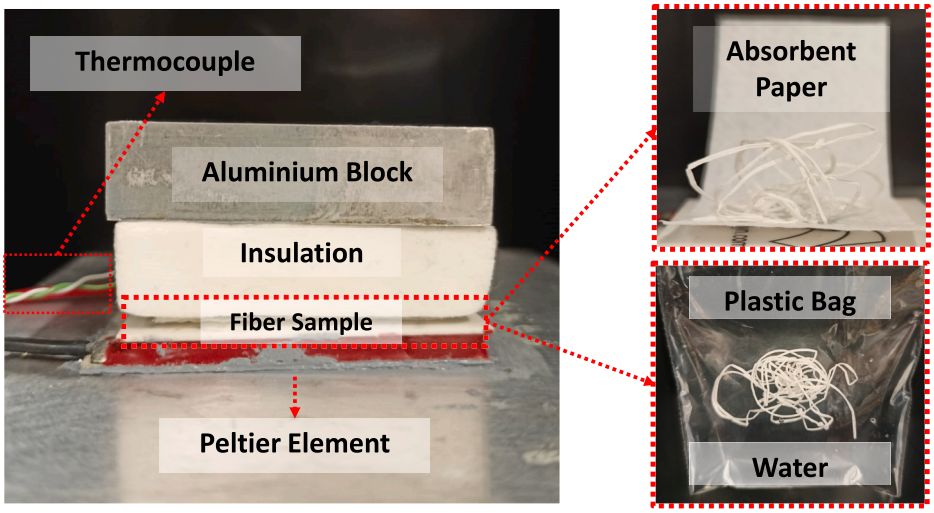

Fig. 2. Thermal cycling setup and fiber sample configurations.

performed within the same temperature range and with the same isothermal periods.

The fiber mass was checked using a Mettler Toledo ML304T/00 balance with the accuracy of 0.4 mg at the beginning of the test and after 50, 100 and 1000 cycles to quantify PCM leakage. Moreover, the fiber enthalpy was evaluated by DSC before the test and both after the 1000 cycles in air and the 500 cycles in water.

2.4.8. *Mechanical properties*

Tensile stress and strain of the PVDF fibers were measured using an Instron 34SC-5 single column universal testing machine with a 100 N capacity sensor. Single fibers were placed between the machine clamps with the help of paper "supports/holders". The measurements were carried out at room temperature with a fixed initial gauge length of 20 mm and a stretching rate of 10 mm/min. Measurement accuracy of the column is ±0.5 % for load and ± 0.02 mm or 0.15 % of total displacement (whichever is greater) for strain values. To obtain an average value, five samples of each fiber were tested.

2.4.9. *Thermal conductivity*

Thermal conductivity of the materials (pelleted PVDF, PCM, and $PVDF_{PCM}$-7.5 fiber) was characterized by means of the transient plane source (TPS) also known as the hot disk method [33]. The size of the sensor and samples, the heating power, and the measurement time were carefully chosen according to the norm Hot Disk ISO 22007-2:2015 [34]. The samples were first prepared as pellets (cylindrical-shaped, diameter: 13 mm, thickness: ca. 4 mm) by pressing them in a hydraulic press at 1 ton for 60 s. All the measurements were carried out using a Kapton 7577 sensor (radius 2.001 mm) subjected to a heating power of 15 mW for a period of 80 s. The recorded data were processed using the Hot Disk Software (version 7.4.0.10).

3. Results and discussion

Firstly, the effect of PVDF concentration in the precursor solution on the morphology, crystallinity, thermal stability, and mechanical properties of pure PVDF fibers, without the presence of PCM, was studied. Next, the effect of PVDF concentration on the encapsulation process of PCM, as well as on the performance and characteristics of final PCM fibers, was analyzed.

3.1. *Effect of polymer concentration on the pure PVDF fibers*

3.1.1. *Morphology*

The surface and cross-section images of the fibers are presented in Fig. 3. The outer surface of the fibers is formed by a dense and smooth PVDF layer that does not present visible holes or imperfections, even if some longitudinal folds can be appreciated. These folds, which also appear in the cross-section images, are the consequence of the pressure difference between the fiber inner phase and the water bath during solvent extraction. The fast solvent extraction rate could generate a low-pressure zone inside the fibers, producing these folds and resulting in a less circular shape.

The inner structure of the fibers can be well observed in cross-section images. Fibers PVDF-5 and PVDF-7.5 present an outer shell formed by a dense PVDF layer, followed by a "finger-like" porous inner structure, typically obtained after "nonsolvent induced phase separation (NIPS)" processes [6,15,29]. Additionally, it can be observed that fiber PVDF-7.5 is less flattened than fiber PVDF-5, which could be attributed to the higher PVDF content in the former, that gives place to a denser structure which is more resistant to the mentioned pressure-induced flattening during the solvent extraction process.

The inner structure of fiber PVDF-10 differs from the above-mentioned ones. Even if the outer PVDF shell is also present, the inner phase is mainly formed by a denser spherulitic structure and a few finger-like pores. This structure can be related to the PVDF content on this fiber, which is the highest of all the produced fibers. With such a high polymer content in the precursor, the solution becomes less stable and a solid-liquid solvent extraction by "thermally induced phase separation (TIPS)" starts to be favored. This solvent extraction pathway gives place to dense spherulitic structures instead of finger-like pores [15,35,36].

This way, in fibers PVDF-5 and PVDF-7.5 solvent extraction is happening by NIPS mechanisms while in fiber PVDF-10, with a less stable precursor solution, both NIPS and TIPS mechanisms would be competing during the solvent extraction process.

3.1.2. *Crystallinity*

The crystallinity of PVDF powder and the produced fibers was calculated by comparing the enthalpy of melting obtained by DSC measurements with the enthalpy of melting of pure PVDF crystals. The thermograms showing the melting process of the samples during a heating ramp from 20 to 200 °C are shown in Fig. 4, while their melting temperature (T_m), associated melting enthalpy (ΔH_m), and the calculated equivalent crystallinity are presented in Table 2.

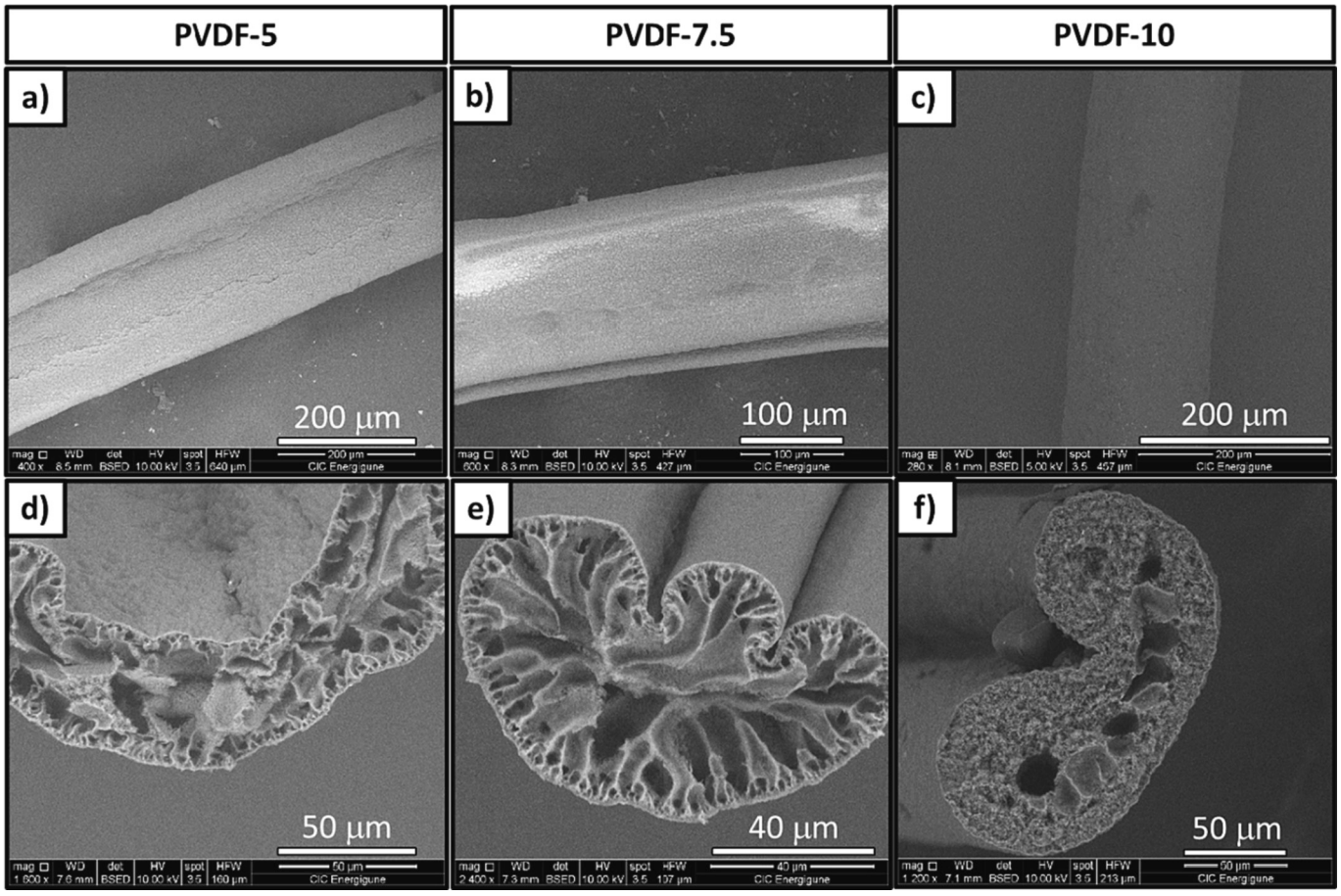

Fig. 3. Surface (a,b,c) and cross-section (d,e,f) images of the PVDF fibers.

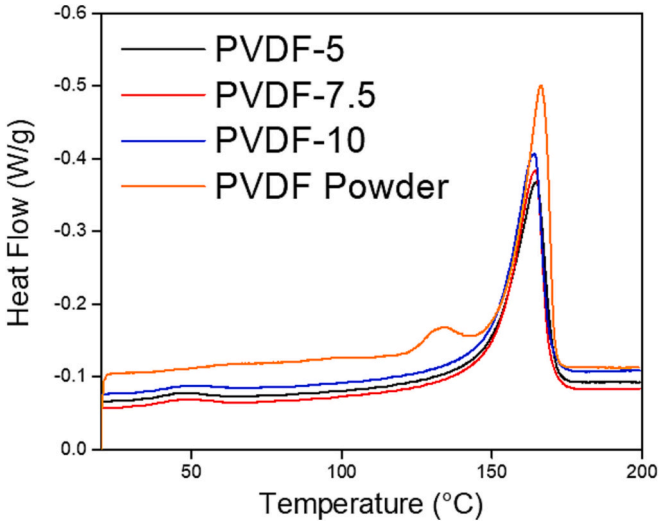

Fig. 4. DSC thermograms of pure PVDF powder and PVDF fibers.

The peak corresponding to the melting of PVDF powder takes place at 167.1 °C with an associated enthalpy of 64.2 J/g. Considering the reference value of 104.7 J/g that corresponds to the melting enthalpy of pure PVDF crystals, the equivalent crystallinity of PVDF powder is 61.3 %.

In the case of fibers, all of them show similar characteristics with melting temperatures ranging between 164.1 and 164.8 °C and associated enthalpies in the range of 52.6 and 53.6 J/g, which correspond to crystallinity values from 50.2 to 51.2 %. All these values are lower than the ones corresponding to PVDF powder, what could be attributed to the fast solvent extraction process. Even so, it must be noted that despite the different polymer concentrations used to produce the different fibers, their final crystallinity is almost the same, which is in accordance with the observed effect by other authors to produce PVDF membranes by solvent extraction method [35].

Table 2
Melting temperature (T_m), melting enthalpy (ΔH_m) and calculated crystallinity of PVDF powder and the PVDF fibers.

Sample	T_m (°C)	ΔH_m (J/g)	Crystallinity (%)
PVDF Powder	167.1	64.2	61.3
PVDF-5	164.8	52.6	50.2
PVDF-7.5	164.6	53.6	51.2
PVDF-10	164.1	53.1	50.7

The PVDF crystalline structure is composed of different phases, the nonelectroactive α phase, and the electroactive β and γ phases. It is well known that phase distribution in PVDF materials can affect their piezoelectric, dielectric, and mechanical properties [37–39]. It is hence expected that it can also influence the thermal stability of the material. Therefore, pure PVDF and the produced PVDF fibers were analyzed by means of FT-IR (Fig. 5) and the relative fractions of β + γ phases (F_{EA}) and α phase (100 – F_{EA}) were calculated (Table 3) by the following Eq. (1) [40]:

$$F_{EA} = \frac{I_{EA}}{\left(\frac{K_{840^*}}{K_{763}}\right) I_{763} + I_{EA}} \times 100\% \quad (1)$$

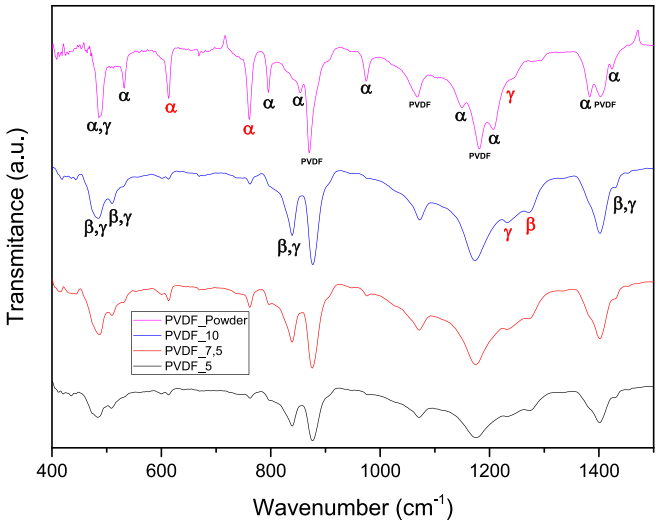

Fig. 5. FT-IR spectra of the PVDF powder and the PVDF fibers.

Table 3
Calculated crystalline phase relative fraction values of the PVDF powder and PVDF fibers.

Sample	α fraction (%)	β + γ fraction (%)
PVDF powder	68.5	31.5
PVDF-5	27.3	72.7
PVDF-7.5	32.4	67.6
PVDF-10	21.7	78.3

where I_{EA} and I_{763} are the absorbances at 840* and 763 $cm^{-1,}$ respectively. K_{840*} and K_{763} are the absorption coefficients at the respective wave numbers, whose values are 7.7 × 10^4 and 6.1 × 10^4 cm^2 mol^{-1}, respectively [41].

From the spectra in Fig. 5, the pure PVDF powder and all the produced PVDF fibers present the characteristic absorption peaks around 881, 1071, 1176 and 1401 cm^{-1}, which are representative of any PVDF sample, but that are not helpful for the determination of the different crystalline phases, as they appear for all the three cases (α,β and γ). Therefore, the exclusive peaks of each crystalline phase need to be considered [40].

The pure PVDF power shows two well defined peaks at 614 and 763 cm^{-1} which are exclusive for α phase. Moreover, several smaller peaks at 532, 795, 854, 975, 1149, 1209, 1383 and 1423 cm^{-1} which correspond also to α phase are present in this sample. It needs to be noted that a little peak at 1234 cm^{-1} can be observed, which is exclusive for γ phase, and that could be related to the peaks at 482–489 cm^{-1} that are usually induced by the presence of both, α and γ phases. Therefore, this spectrum indicates that PVDF powder is mostly formed by α phase crystals with little contribution from the other two phases.

On the other side, PVDF fibers present a different spectrum. The α phase exclusive peaks that were present in the powder almost disappear, leaving only small peaks at 535, 614, 763, 795 and 975 cm^{-1}. Instead, the peak at 1234 cm^{-1} exclusive for γ phase has increased and a new peak at 1275 cm^{-1} has appeared, which is exclusive for β phase. This, as well as the presence of new dual peaks in the ranges of 473–482 cm^{-1}, 1429-14,031 cm^{-1} and the peaks at 510 and 840 cm^{-1} indicate a great contribution of β and γ phases in the PVDF fiber's crystalline structure.

As seen, the crystalline structure of PVDF transforms from an α phase predominant state to a β + γ predominant structure. To quantify the relative fraction of each of the phases, Eq. (1) has been used, which considers the absorbance values at 763 cm^{-1} (related to α phase) and 840 cm^{-1} (related to β + γ phases). The obtained values are presented in Table 3.

The relative fraction values from Table 3 support the analysis of the FT-IR spectra, indicating that the β + γ phases relative contribution on the crystalline structure of the fibers is more than double of the relative fraction in the PVDF powder, with values above 67 % in all the fibers. This α to β + γ transformation is typically obtained by controlling different parameter in PVDF film, membrane, and filament production methods [42–46].

3.1.3. Thermogravimetric analysis (TGA)

TGA was carried out with the aim of evaluating the thermal stability of the PVDF fibers. The obtained TGA and DTG profiles for PVDF powder and fibers are presented in Fig. 6, while the initial mass loss temperature (corresponding to a mass loss of 5 %), maximum degradation temperature and final residue values are gathered in Table 4.

The obtained results show that all the PVDF fibers start to suffer thermal degradation at lower temperatures than the pure PVDF powder. Fibers PVDF-5 and PVDF -7.5 show nearly identical thermal stability, while fiber PVDF-10 presents higher degradation temperatures. This is related with the higher β crystalline phase contribution in fiber PVDF-10, that is helping to increase its thermal stability, because of the better molecular packaging of this crystalline phase [47,48]. Moreover, the denser structure and absence of finger like pores due to the contribution of TIPS mechanism could also be boosting this fiber against thermal degradation.

Finally, it needs to be mentioned that PVDF powder presents higher thermal stability than any of the produced fibers, what could be related to the higher crystallinity degree shown by the powder. Even so, all the fibers are completely stable below 300 °C, which is enough for their combination with PCMs for applications like thermal management and thermal comfort.

3.1.4. Mechanical properties

Resistance against stretching and elasticity are key properties of fibers whose purpose is to fit textile applications or to produce fabrics intended for other applications. For that issue, the mechanical properties of the fibers were measured by tensile stress tests. The measured average elastic modulus, stress at breakpoint, and elongation at breakpoint of each type of fiber are gathered in Fig. 7.

Firstly, fiber PVDF-5 presents an elastic modulus of 2.40 mN/Tex, a breakpoint stress of 11.70 mN/Tex and a maximum average elongation of 264.3 %. As the polymer concentration and the β crystalline phase contribution on the fibers increases, so does their mechanical strength [49–51]. This is the case of fiber PVDF-7.5, whose elastic modulus and stress at breakpoint increase to 4.16 mN/Tex and 14.90 mN/Tex, respectively, even if its maximum elongation decreases to 213.8 %, which is 19 % lower than for fiber PVDF-5.

In the case of fiber PVDF-10, that has the highest polymer concentration, the breakpoint stress increases even more, reaching 19.43 mN/Tex, while the elastic modulus reaches the value of 4.22 mN/Tex, which is slightly higher than for PVDF-7.5. Moreover, the elasticity of the fiber presents a huge increase, with a maximum elongation of 522 %, which is almost two times the elongation of fibers PVDF-5 and PVDF-7.5.

This elasticity enhancement, that did not happen with the increase of PVDF from 5 % to 7.5 %, can be attributed to the elimination of the finger-like pores promoted by the TIPS mechanism that gives rise to the inner structure of fiber PVDF-10 which is much denser and lacks on macrovoids that can hinder mechanical properties of the fiber [35]. Thus, the increase of the polymer content in the precursors leads to the formation of fibers with denser structures, better thermal stability and enhanced mechanical properties. Regarding the last, they are expected to be preserved in the $PVDF_{PCM}$ fibers, as previous studies have demonstrated that the encapsulation of PCMs into PVDF fibers by this method does not influence their mechanical properties in a noticeable way [30].

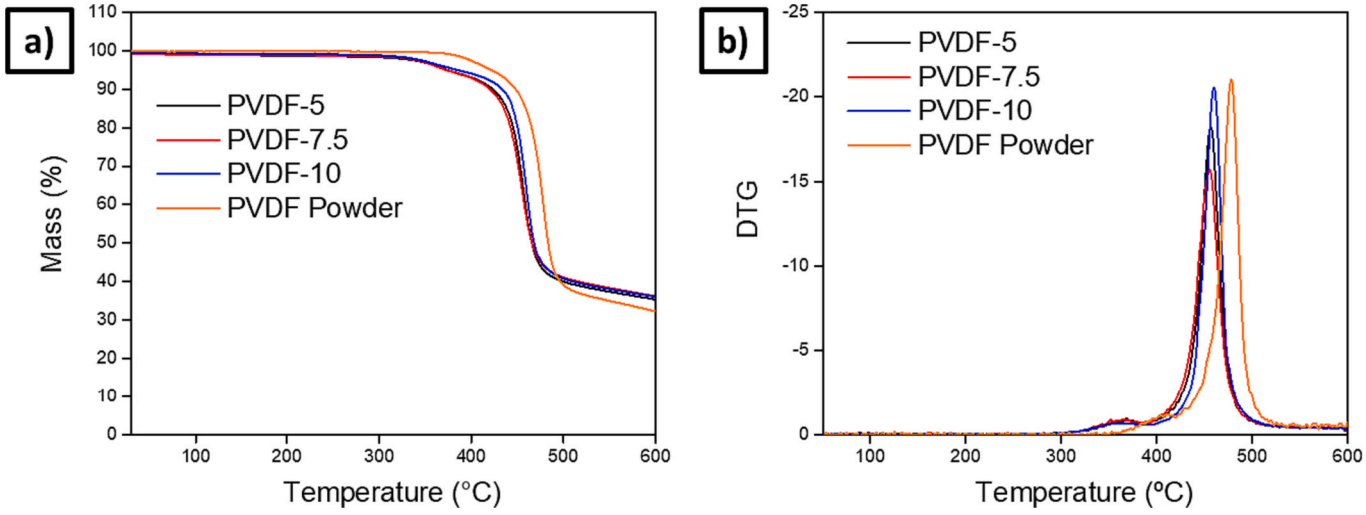

Fig. 6. TGA (a) and DTG (b) profiles of the PVDF powder and the PVDF fibers.

Table 4
Degradation temperature and residue values of the PVDF powder and the PVDF fibers.

Sample	T(−5 %)	T_{max} (°C)	Residue (%)
PVDF-5	373.3	456.6	35.5
PVDF-7.5	372.3	455.6	36.3
PVDF -10	384.5	460.0	36.2
PVDF Powder	421.6	478.2	32.3

3.2. *Effect of polymer concentration on the PCM encapsulation*

3.2.1. *Droplet size of the precursor emulsions*

The enthalpy of the fibers produced by the emulsion jet-injection method is limited by the homogeneity and stability of the precursor emulsion. This emulsion consists of a solvent, a polymer and the PCM to be encapsulated, and is very susceptible to destabilization and coagulation due to the high solvent extraction rates involved in this process, resulting in PCM losses [30]. For this reason, the droplet size of the precursor emulsions used to produce $PVDF_{PCM}$ fibers has been studied as soon as they were formed. Droplet size distributions are presented in Fig. 8.

The 5 % and 7.5 % PVDF precursors present a smaller and more homogeneous emulsion size than the 10 % PVDF precursor. The average droplet sizes for the 5 % and 7.5 % PVDF emulsion are 12.0 and 10.3 μm, respectively, with minimum droplet sizes of 2 μm and maximum droplet sizes of 40 μm. On the other hand, the 10 % PVDF emulsion has a mean droplet size of 46.4 μm, a minimum droplet size of 8 μm and a maximum droplet size of 160 μm.

These variations in droplet size with the increase of PVDF concentration can be attributed to the viscosity of the precursors and the energy required to form the emulsions. It is known that the viscosity of PVDF solutions increases exponentially with polymer concentration [52], with the viscosity of the 10 % PVDF precursor being much higher than that of the rest.

In this sense, the increase of the PVDF from 5 % to 7.5 % increases slightly the solution's viscosity. This favors the emulsion stability and gives as a result a lower average droplet diameter. On the contrary, the increase of PVDF content to 10 % results in a too high viscosity and becomes detrimental for the emulsion formation. Since the method of preparation of the precursors has been the same in all three cases, the energy used has been the same. Thus, in the 10 % PVDF precursor, the energy applied would not have been sufficient to emulsify the PCM as homogeneously as in the rest of the precursors, giving rise to a more heterogeneous emulsion with larger droplet size.

3.2.2. *Morphology*

Fig. 9 shows surface and cross-section images of the $PVDF_{PCM}$ fibers. Moreover, with the aim of studying in deep the internal structure of the fibers and the distribution of the PCM inside them, longitudinal section

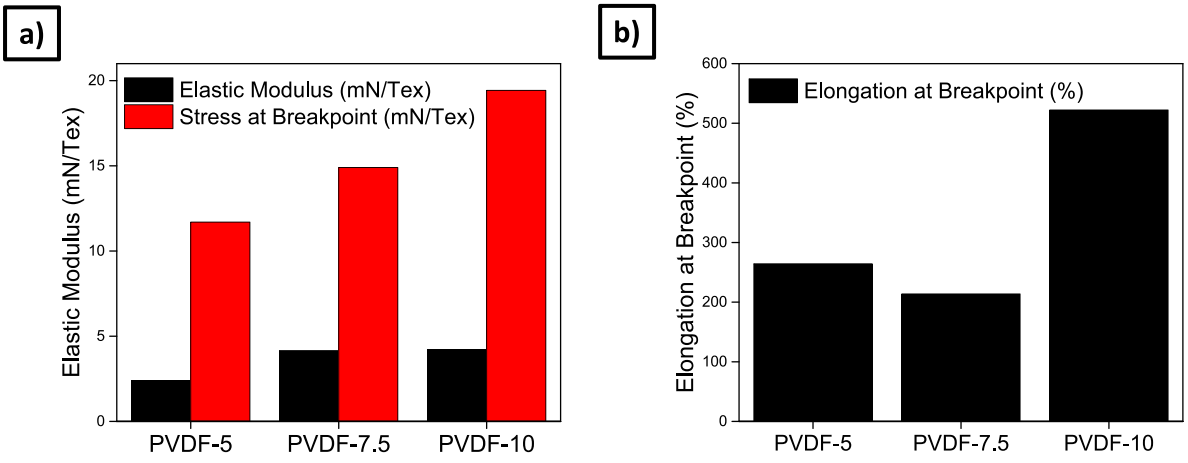

Fig. 7. a) Average elastic modulus, stress at breakpoint and b), elongation at breakpoint of the PVDF fibers.

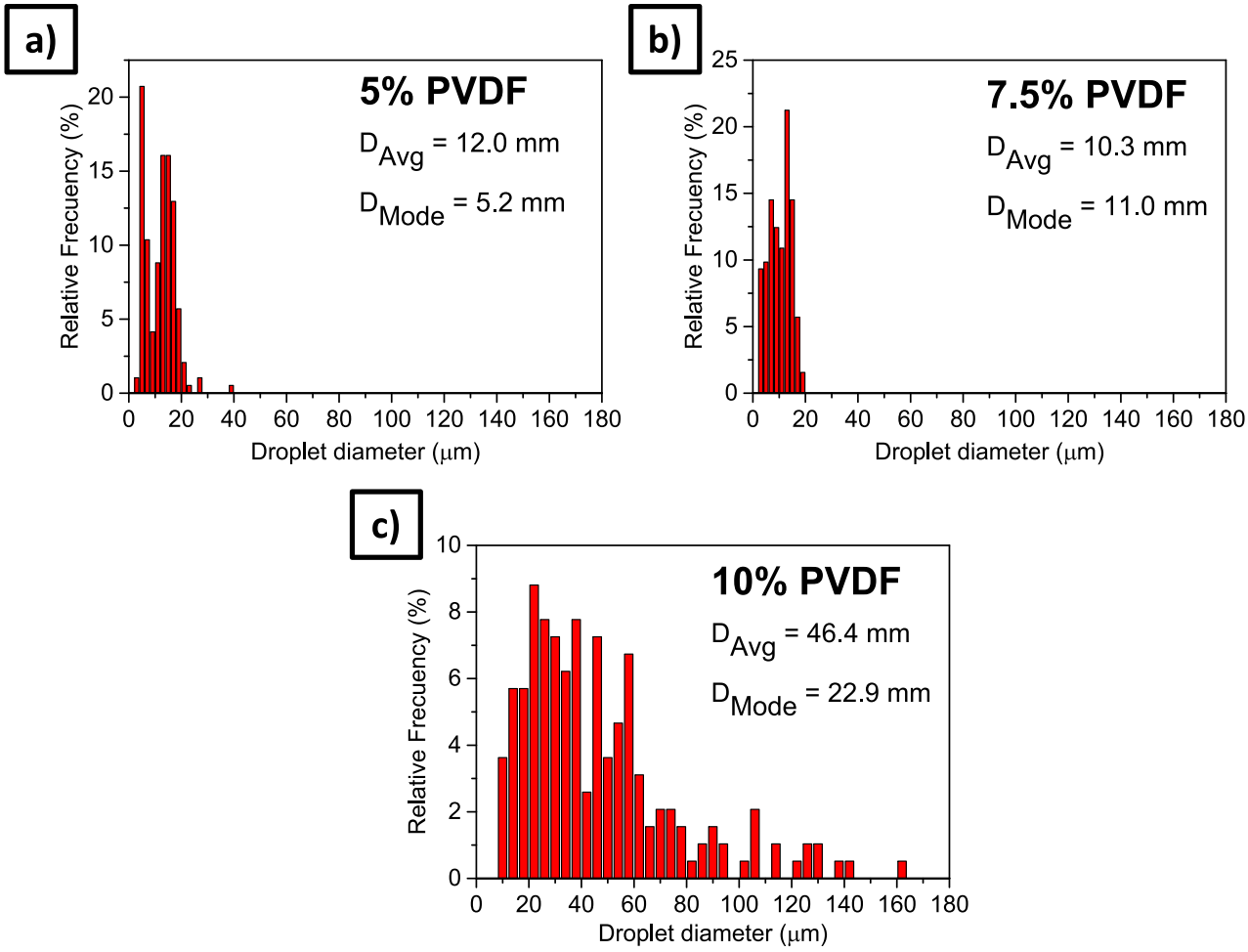

Fig. 8. Droplet size distribution of the emulsions prepared with a) 5 %, b) 7.5 % and c) 10 % PVDF precursors.

images are also presented.

The surface of the $PVDF_{PCM}$ fibers is dense and presents no imperfections (Fig. 9 a,b,c), as happened for the pure PVDF fibers. Nonetheless, some morphological differences can be appreciated in the cross section of the fibers (Fig. 9 g,h,i). $PVDF_{PCM}$ fibers present a less flattened shape with less longitudinal folds than pure PVDF fibers. This is promoted by the presence of PCM, that acts as support for the fiber wall and prevents severe folding during solvent extraction.

On the other side, $PVDF_{PCM}$ fibers present a dense PVDF layer in the outer side followed by a porous structure with increasing pore size towards the center of the fibers, where the biggest cavity is located. This morphology is typical for solvent extraction processes and was also observed in fibers produced in our previous work. Moreover, this pore distribution resulted beneficial for PCM encapsulation, as the PCM could be stored in the big pores, while the lower sized ones increased the capillary forces inside the fibers, preventing PCM leakage [30]. It must be pointed out that this central cavity is smaller for fiber $PVDF_{PCM}$-7.5 (Fig. 9 h) than for $PVDF_{PCM}$-5 (Fig. 9 g) and disappears in some points of fiber $PVDF_{PCM}$-10 (Fig. 9 i), which is a result of the increasing PVDF concentration in the precursors. In the specific case of $PVDF_{PCM}$-10, the appearance of solid zones can also be related to the high viscosity of the precursor and heterogeneity of the emulsion, which can promote PCM-free zones in the jet during the injection process.

In our previous work, it was observed that the fibers produced by this pathway presented a non-homogeneous distribution of the PCM, that was distributed in slugs all along the fibers structure. Images of the longitudinal section allow us to see the internal structure of the fibers, giving us an idea of the "free space" where the PCM can be distributed. In those images can be seen that fiber $PVDF_{PCM}$-5 (Fig. 9 d) presents cavities with a wide size distribution along its structure. On the other side, the fibers with higher PVDF content present denser structures with a much more homogeneous cavity distribution, being fiber $PVDF_{PCM}$-7.5 (Fig. 9 e) the most homogeneous. Nevertheless, even if the presence of the PCM can modify the fibers internal shape, the FT-IR analysis has shown that there is not a chemical interaction between the two materials during fiber production, as no new peaks appeared in the diffractograms (See Fig. S1 from supplementary information).

3.2.3. *DSC analysis*

As seen before, the content of PVDF affects the size and stability of the precursor emulsions and thus, may affect the PCM content and distribution inside the fibers. For the analysis of these parameters, six samples of each $PVDF_{PCM}$ fiber have been analyzed by DSC. The average values of melting point, associated enthalpy, PCM content, and PCM variability are presented in Table 5, while Fig. 10 shows the most representative thermograms of each fiber.

Considering the values from Table 5, in general the $PVDF_{PCM}$ fibers present an exothermic peak associated to the melting process of the PCM with an onset point between 21.2 and 22.9 °C, increasing with the PVDF content and being in the range of 0.1 and 1.8 °C higher than the melting point of the PCM.

Paraffin RT-25HC exhibits its melting point at 25 °C with an onset temperature of 21.1 °C. This is conditioned by the effect of a solid-solid transition prior to melting of this material and that is a common behavior for paraffins [53]. These two transitions are more evident in the cooling step. The crystallization of RT-25HC presents an onset

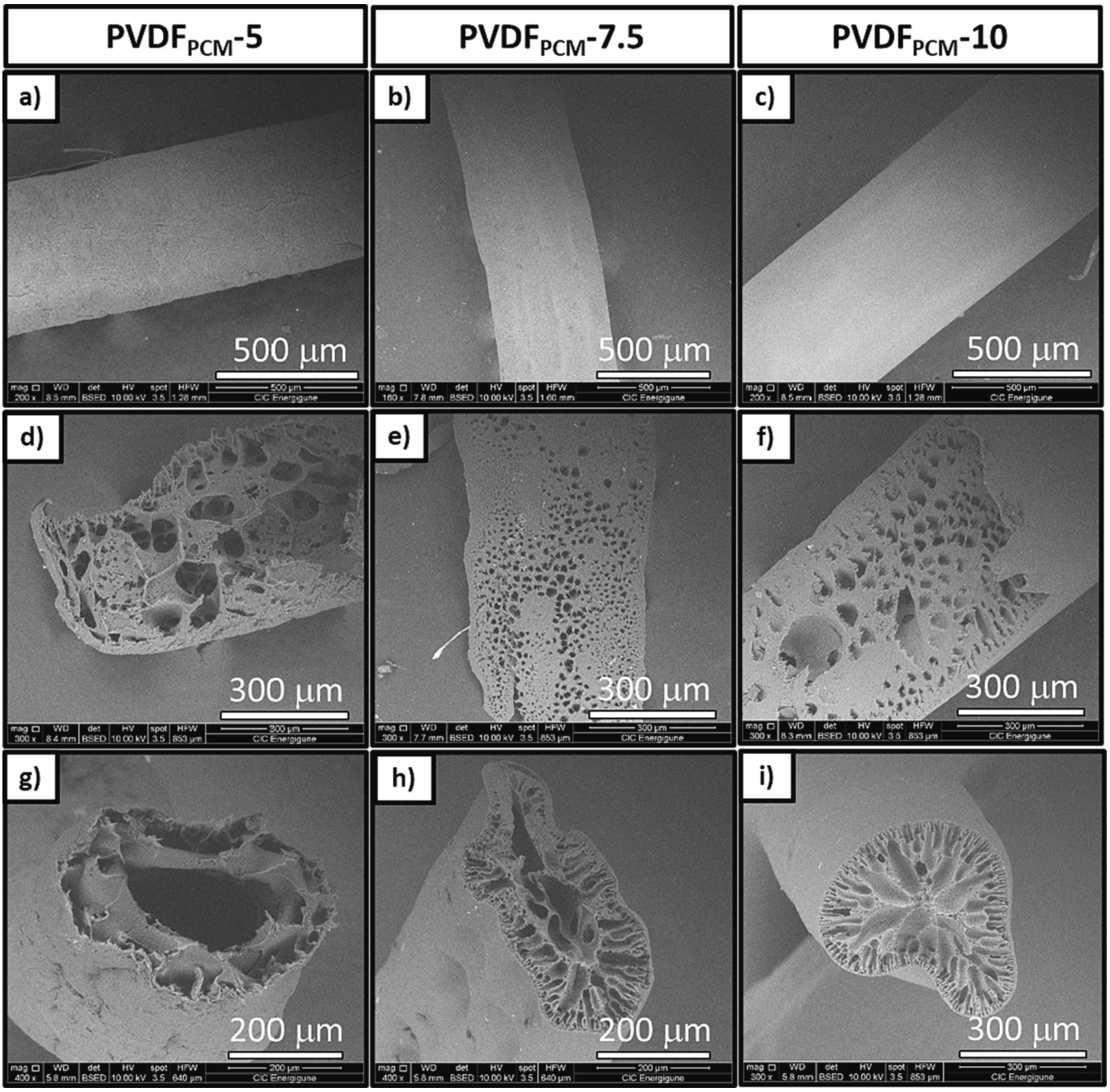

Fig. 9. Surface and cross-section images of the PVDF$_{PCM}$ fibers.

Table 5
Melting point, associated enthalpy and PCM content values of the PVDFPCM fibers.

Sample	Av. Mp (Onset) (°C)	Max. ΔH (J/g)	Min. ΔH (J/g)	Av. ΔH (J/g)	PCM content (wt%)	
					Average value	Standard deviation (%)
RT25HC	21.1	–	–	201	–	–
PVDF$_{PCM}$-5	21.2	81	44	62	31.0	22.7
PVDF$_{PCM}$-7.5	22.2	137	108	127	63.5	6.1
PVDF$_{PCM}$-10	22.9	46	28	37	18.3	14.5

temperature at 23 °C, while its reverse solid-solid transition starts at 16 °C, indicating 5 °C of subcooling. Nevertheless, this effect is diminished when the PCM is encapsulated in the fibers, as they present a single peak in the cooling stage.

On the one side, the melting enthalpy values are different for each fiber, as well as the average core content. Fiber PVDF$_{PCM}$-5 presents an average melting enthalpy of 62 J/g, that is equivalent to an average core content of 31 %. Nevertheless, the enthalpy values vary in the range of 81 and 44 J/g. On the other side, fiber PVDF$_{PCM}$-7.5 presents enthalpy values between 108 and 137 J/g, with an average of 127 J/g, which implies an average core content of 63.5 %. This core content is the highest for all the produced fibers. Furthermore, it is worth noting that the enthalpy values obtained for this fiber are the highest reported to date for polymeric fibers with encapsulated PCMs produced by microfluidic approaches. Finally, the enthalpy values of fiber PVDF$_{PCM}$-10 are

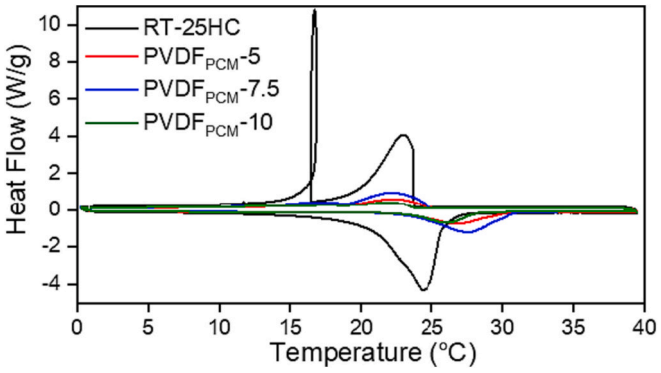

Fig. 10. DSC thermograms of the raw PCM and the PVDF$_{PCM}$ fibers.

in the range of 28 and 46 J/g, with an average value of 37 J/g, which gives an average core content of 18.3 %.

As mentioned, the enthalpy values of the fibers present a variation, which indicates that the PCM is non-homogeneously distributed along the structure of the fiber [30]. The variability of the enthalpy values of each fiber (calculated as the relative standard deviation of the enthalpy values) is presented in Fig. 11. The variability of fibers PVDF$_{PCM}$-5 %, PVDF$_{PCM}$-7.5 and PVDF$_{PCM}$-10 are 22.7 %, 6.1 % and 14.5 % respectively.

The enthalpy values and the variability of the PCM within each fiber are influenced by the droplet sizes observed for each of the precursors. In the case of the 10 % PVDF precursor, the droplet size distribution was very wide and with a larger average size than the other precursors. Such large droplets can easily escape from the precursor jet during the injection process if they are located at the edges of the jet [30] or even coalesce to form even larger droplets, generating a phase separation in the jet that gives rise to zones of pure polymers and pure PCM. This explains the presence of some solid zones in the PVDF$_{PCM}$-10 fiber (Fig. 9 i) and the discontinuous fiber production observed during the production process.

On the other hand, although the droplet sizes of the 5 % and 7.5 % PVDF precursors are very similar, the PVDF$_{PCM}$-5 fibers have shown significantly lower PCM content and higher PCM variability. This is related to the viscosity of the precursors, which, as already mentioned, increases considerably with increasing polymer concentration. Thus, despite having a very similar size before the injection process, it is possible that the emulsion of the 5 % precursor tends to destabilize and coagulate during fiber production, leading to the formation of larger droplets that generate PCM losses and a less homogeneous distribution, as it happens for the 10 % PVDF precursor.

As summary, even if the increase of polymer concentration has shown to be beneficial to produce pure PVDF fibers, its benefits for the encapsulation of the PCM are limited by the viscosity of the polymer solutions, resulting to be prejudicial upon certain point. In the case of the 7.5 % precursor, its viscosity favors a good emulsion size and stability, helping to retain the PCM within the jet during fiber formation and resulting in a higher and more homogeneous PCM content. This fiber presents enthalpy values up to 137 J/g, an average PCM content of 63.5 %, and a PCM variability of 6.1 %, which are overpassing the limitations found for this method in our previous work (max 98 J/g, 33 % PCM and 13 % variability) and indicate that can be competitive with other more complex methods in terms of latent heat and PCM content.

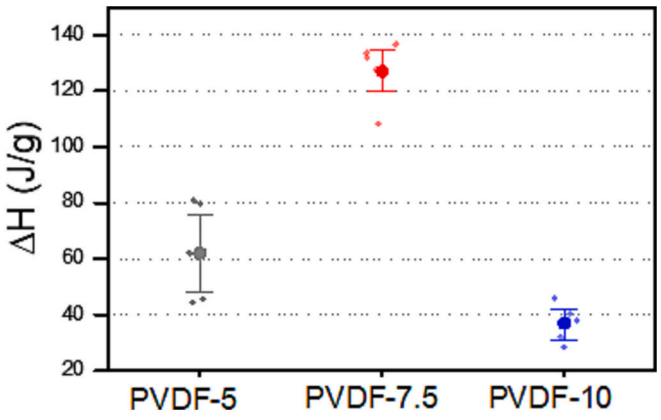

Fig. 11. Enthalpy value range of the PVDF$_{PCM}$ fibers.

3.2.4. *Thermogravimetric analysis (TGA)*

The TGA and DTG profiles of the PVDF$_{PCM}$ fibers, PVDF powder and the raw PCM are shown in Fig. 12, while the degradation temperatures, mass losses, and residue values are compiled in Table 6.

The PCM used in this work is thermally stable up to 181.4 °C, when its thermal decomposition starts, reaching a maximum degradation point at 271.3 °C and leaving almost no residue at 600 °C. On the other side, the PVDF$_{PCM}$ fibers present 2 main thermal degradation peaks. The first one is associated with the encapsulated PCM, which starts to decompose at 175.9 °C, 172.9 °C and 193.5 °C for the fibers PVDF$_{PCM}$-5, PVDF$_{PCM}$-7.5 and PVDF$_{PCM}$-10 respectively. These temperatures are between 6 °C lower and 12 °C higher than the raw PCM and still far above its working temperature. Fiber PVDF$_{PCM}$-10 shows the best thermal stability of the PCM, which is a consequence of the lower PCM content and the denser structure of this fiber. The highest mass loss is 58.9 % for fiber PVDF$_{PCM}$-7.5, which is in accordance with the average PCM contents calculated from DSC analysis. The second degradation peak is associated to the polymeric part of the fibers, which thermally decomposes at temperatures between 444.5 °C and 477.4 °C.

3.2.5. *Thermal conductivity*

The values of thermal conductivity obtained by the Hot Disk method are presented in Table 7. The PVDF and paraffin pellets have thermal conductivities of 0.189 and 0.425 W/m K, respectively, while the PVDF$_{PCM}$-7.5 fiber pellet has a thermal conductivity of 0.371 W/m K. This last results is in agreement with the conventional series and parallel mixture rules [54] which lead to a thermal conductivity ranging between 0.333 and 0.373 W/m K for the PVDF$_{PCM}$-7.5 fiber pellet.

The thermal conductivity presented by the PVDF$_{PCM}$-7.5 fiber is higher than those measured for the fibers produced in our previous work, which was 0.287 W/mK [30], even though the paraffin used in that case had a thermal conductivity of 0.571 W/mK, which is higher

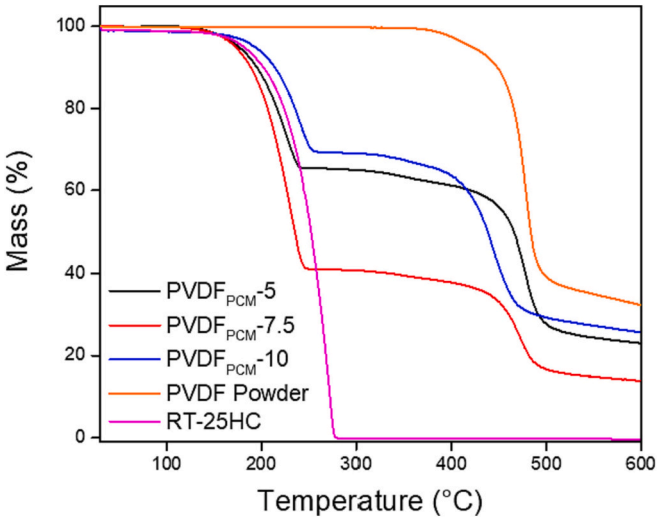

Fig. 12. a) TGA and b) DTG profiles of the pure PCM, PVDF powder and the PVDF$_{PCM}$ fibers.

Table 6
Degradation temperature and mass loss values of the pure PCM, PVDF powder and $PVDF_{PCM}$ fibers.

Sample	T (−5 %)	T1 (°C)	Loss 1 (%)	T2 (°C)	Loss 2 (%)	Residue (%)
$PVDF_{PCM}$-5	175.9	227.7	34.6	477.4	36.9	23.0
$PVDF_{PCM}$-7.5	172.9	230.1	58.9	472.1	22.7	13.9
$PVDF_{PCM}$-10	193.5	240.6	29.7	444.5	41.4	25.7
RT-25HC	181.4	271.3	99.2	x	x	0.4
PVDF_Powder	421.6	x	x	478.2	62.9	32.3

Table 7
Thermal conductivity of pure PVDF, RT-25HC and $PVDF_{PCM}$-7.5 fiber.

Sample	Therm.Cond. (W/m·K)	Ave. Dev. (W/m·K)	Ave.Dev. (%)
PVDF	0.189	0.001	0.5
RT-25HC	0.425	0.019	4.5
$PVDF_{PCM}$ − 7.5	0.371	0.026	7.0

than the one of the current PCM. This thermal conductivity increase is related to the PCM content that is encapsulated in each of the fibers, which was an average of 34 % in the previous work and 63.5 % in the current fibers. Therefore, the higher amount of PCM encapsulated in these new fibers helps to enhance their thermal conductivity.

3.2.6. *Cyclability and leakage*

Apart from the PCM content and enthalpy, other important properties determine the viability of the final fibers for their use in thermal management and thermal buffering systems. This is the case of PCM retention capacity and cyclability, which indicate if the fibers can overcome several working cycles above and below the PCMs melting point without leakage or enthalpy loses. From bibliography, most of the work done to evaluate the PCM retention capacity and cyclability of the polymeric fibers with encapsulated PCMs is based on cycling test performed with a DSC (from 5 to 100 cycles) [6,15–17,22,29] or leakage tests that are performed under isothermal conditions.

To analyse the capacity of the produced fibers of overcoming working heating/cooling cycles, fiber $PVDF_{PCM}$-7.5 was submitted to continuous cycling between 10 and 40 °C on different cycling tests. This fiber was selected for this analysis as it was the one with the best properties in terms of latent heat and PCM content.

On the one side, the fiber was submitted to 100 cycles in the DSC. As can be seen in Fig. 13, where the resultant thermograms of cycles 1, 50 and 100 are presented, the fiber shows no change in melting temperature and associated enthalpy, being these values of 22 °C and 120 J/g respectively. This result indicates that, following the most frequently used methodology for thermal cycling, the fiber is completely stable after 100 cycles.

Nevertheless, cycling by DSC gives information about the repeatability of the PCMs performance under "inert" conditions but does not allow checking whether the PCM is leaking from the fibers or not. On the other side, leakage tests at constant temperature allow to evaluate the stability of the fibers at certain temperature, but do not evaluate the "aging" of the fibers during and after several work cycles, which is more stressful and closer to the fiber's real behavior in the final application. Moreover, leakage tests are done in "dry" atmosphere, but is also interesting to evaluate the performance of the fibers under external agents like water, as in some of their potential applications (textiles) they may be exposed to rain or even immersed in water.

Thus, to acquire more realistic information about the capability of the fiber to withstand working thermal cycles, it was submitted to a more "exigent" cycling test. The mass, enthalpy and PCM content of the fiber was measured after each part of the cycling test, and the main relevant results are presented in Fig. 14.

The first part of this cycling test consisted in cycling the fiber in open

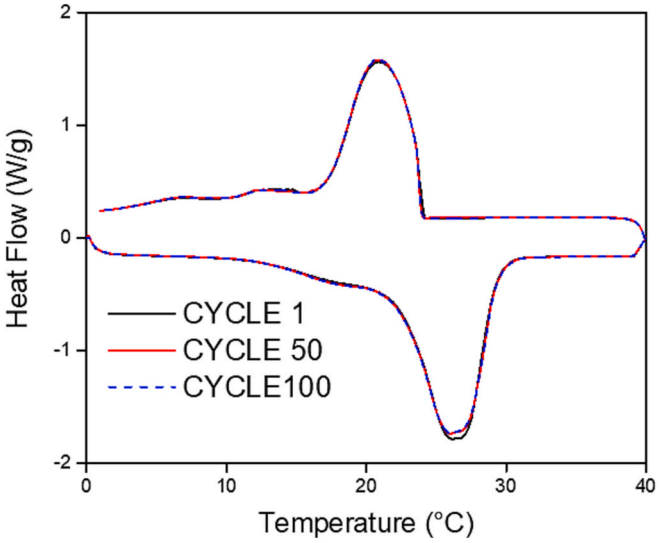

Fig. 13. DSC thermograms of fiber $PVDF_{PCM}$-7.5 on cycles 1, 50 and 100.

atmosphere under little pressure and being in contact with absorbent paper for extracting any PCM that could leak during the test. The mass loss of the fibers was 1 wt% after the first 10 cycles, 2.5 wt% after 100 cycles and 8.5 wt% after 1000 cycles.

The second part of the cycling test consisted in immersing the same fiber sample into water and cycling it again for 500 times. No mass loss occurred during the first 20 cycles, the loss after 100 cycles was 1.9 wt% and the final loss after 500 cycles reached 7.7 wt%.

After the 1000 cycle test in air, the average enthalpy of the fiber decreased from 117 to 92 J/g, which represents an enthalpy loss of 21 %. Moreover, after the 500-cycle test in water, the enthalpy was reduced to 75 J/g, indicating an additional enthalpy loss of 15 %.

The thermal stability of the fiber is not affected by thermal cycling or exposure to water since the fiber remains stable up to approximately 170 °C and shows its maximum degradation between 220 and 230 °C as the uncycled fiber does. Nevertheless, the PCM content in the fibers decreases in accordance with their enthalpy, going from 59 % to 48 % after the 1000 cycles in air, and decreasing to 40 % after the additional 500 cycles in water.

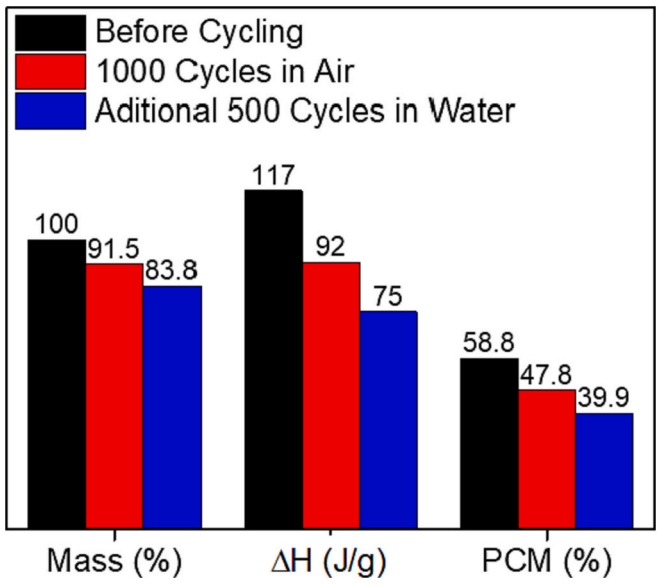

Fig. 14. Evolution of the mass, enthalpy and PCM content of fiber $PVDF_{PCM}$-7.5 after thermal cycling tests.

Finally, the FT-IR analysis has shown that there is no chemical interaction between the PCM and the PVDF during thermal cycling (See Fig. S1 from Supplementary information). Nevertheless, the peaks corresponding to the PCM appear more evidently after cycling, suggesting that it is located closer to the surface of the fibers. This is in accordance with the results observed in our previous work [30]. The porous structure of the fibers allows the PCM to spread when it is in molten state, therefore allowing it to allocate closer to the fiber walls and intensifying its FT-IR peaks.

Moreover, the freedom of the PCM to move through the porous structure limits the volumetric expansion of the fibers. This is evident when the volumetric thermal expansion of the fiber during the phase change is analyzed (See Fig. S2 from supplementary information). According to the observed data, the maximum expected volumetric expansion is below 4.5 %. This is much lower than the volumetric expansion of the pure PCM, that is 12.5 % given by the suppliers' datasheet.

In summary, these results show that the $PVDF_{PCM}$-7.5 fiber exhibits excellent resistance to thermal cycles around the working temperature of the encapsulated PCM, showing an excellent repeatability of melting temperature and enthalpy. Moreover, it can maintain >78 % of its enthalpy after 1000 cycles in ambient atmosphere and >64 % after cycling in air and exposure to water for additional 500 cycles, all while maintaining the thermal stability, shape and chemical structure of the material. These results are very promising, given that the enthalpy values obtained are in the range of those obtained by other authors with much more "conservative" cycling tests, as can be seen in Table 8.

4. Conclusions

In this work the production of PVDF fibers with encapsulated PCMs by emulsion jet injection method has been optimized by the increase of polymer content as emulsion stabilizer of the fiber precursors. This strategy has shown to favor the production of PVDF fibers with denser structures. Moreover, the increase of PVDF content to 10 % promotes the formation of the fibers by TIPS mechanism, eliminating the finger like pores of the structure and increasing overall the mechanical properties of the fibers.

The increase of PVDF content also affects the viscosity of the precursors, having an impact on the emulsion formation. The increase of PVDF content to 10 % produces a drastic increase of viscosity that hinders the emulsion formation and gives place to heterogeneous emulsion precursors with big droplet sizes, resulting in PCM loses during fiber production and low encapsulation rates.

Nevertheless, the use of 7.5 % PVDF allows the preparation of precursors with an adequate viscosity that favors both emulsion formation and stability. The fiber produced with this strategy showed the best encapsulation results, with an average PCM content of 63.5 wt% and enthalpy values up to 137 J/g, which is the highest enthalpy obtained up to date for fibers produced by microfluidic approaches, all this with a PCM variability of 6 %. To further improve these values, a combination of the current fiber formation method with a simple microfluidic system that allows to control both the PCM and PVDF proportions looks like a promising future step. Nevertheless, the reproducibility of the microfluidic devices needs to be addressed for this purpose. Moreover, this fiber has excellent stability among cycles in DSC and can preserve >64 % of its enthalpy after being submitted to 1500 cycles sequentially in both air and water environments. The effect of thermal cycling on the mechanical properties of the $PVDF_{PCM}$ fibers is intended to be checked in future studies.

Overall, these results show that the emulsion jet injection method can be competitive with other strategies used to produce polymeric fibers with encapsulated PCMs in terms of enthalpy, PCM content and cyclability, while maintaining its advantages like simplicity and use of surfactant-free emulsions.

Table 8
Summary Polymer/PCM fibers submitted to thermal cycling.

Material	ΔH Before (J/g)	Core (%)	Cycles	Method	ΔH After (J/g)	REF
PU/Soy Wax	37	52	100	DSC	37	[17]
PVB/RT-27	109	60	10 / 5	DSC / Air	103 / X	[6]
PVA/ Plant Oil	80	44	100	DSC	79	[22]
PVB/RT-27	117	65	5	Air	X	[29]
PVDF/ Paraffin	79	78	100	DSC	78	[15]
TPU/ PCMs	178	77	50 / 1	DSC / Air	174 / X	[16]
PVDF-RT-25	**120**	**60**	**100**	**DSC**	**120**	**THIS WORK**
PVDF/ RT-25	**117**	**58**	**1000 / 500**	**Air / Water**	**92 / 75**	**THIS WORK**

CRediT authorship contribution statement

Mikel Duran: Writing – review & editing, Writing – original draft, Validation, Methodology, Investigation, Formal analysis, Data curation. **Angel Serrano:** Writing – review & editing, Writing – original draft, Supervision, Methodology, Investigation. **Artem Nikulin:** Writing – review & editing, Writing – original draft, Methodology, Conceptualization. **Jean-Luc Dauvergne:** Writing – review & editing, Writing – original draft, Software, Methodology, Formal analysis, Data curation. **Jalel Labidi:** Writing – review & editing, Supervision, Funding acquisition. **Elena Palomo del Barrio:** Writing – review & editing, Writing – original draft, Visualization, Supervision, Funding acquisition, Conceptualization.

Declaration of competing interest

The authors declare that they have no known competing financial interests or personal relationships that could have appeared to influence the work reported in this paper.

Data availability

Data will be made available on request.

Acknowledgments

Mikel Duran Lopez would like to thank the Department of Education, Linguistic Politics and Culture of the Basque Country government for the granted pre-doctoral contract (PRE_2019_1_0154).

Appendix A. Supplementary data

Supplementary data to this article can be found online at https://doi.org/10.1016/j.est.2024.111032.

References

[1] M. Zare, K.S. Mikkonen, Phase change materials for life science applications, Adv. Funct. Mater. 33 (12) (2023).
[2] X. Zhao, D. Zou, S. Wang, Flexible phase change materials: Preparation, properties and application, Chem. Eng. J. 431 (P2) (2022) 134231 [Internet]. Available from: https://doi.org/10.1016/j.cej.2021.134231.
[3] K. Wang, N. Cai, F. Yu, M. Wang, Bead-like PCM composite network with reinforced heat storage performance for highly efficient battery cooling, J. Energy Storage 54 (July) (2022) 105335 [Internet]. Available from: https://doi.org/10.1016/j.est.2022.105335.

[4] X. Kong, X. Liu, J. Yuan, J. Xu, J. Han, Composite phase change materials with thermal-flexible and efficient photothermal conversion properties for solar thermal management, J. Energy Storage 78 (December 2023) (2024) 110027 [Internet]. Available from: https://doi.org/10.1016/j.est.2023.110027.

[5] J. Shi, M. Qin, W. Aftab, R. Zou, Flexible phase change materials for thermal energy storage, Energy Storage Mater. 41 (May) (2021) 321–342 [Internet]. Available from: https://doi.org/10.1016/j.ensm.2021.05.048.

[6] G.Q. Wen, R. Xie, W.G. Liang, X.H. He, W. Wang, X.J. Ju, et al., Microfluidic fabrication and thermal characteristics of core-shell phase change microfibers with high paraffin content, Appl. Therm. Eng. 87 (2015) 471–480.

[7] J.M. Laza, A. Veloso-Fernández, J. Sanchez-Bodon, A. Martín, A.M. Goitandia, C. Monteserín, et al., Analysis of the influence of microencapsulated phase change materials on the behavior of a new generation of thermo-regulating shape memory polyurethane fibers, Polym Test. 116 (June) (2022).

[8] L. Hu, J. Chen, J. She, F. Li, J. Liao, Y. Zhou, et al., A hierarchical core-sheath structure composite fiber of PW/TPU towards elastic smart thermal management fabrics, J. Energy Storage 77 (December 2023) (2024) 109802 [Internet]. Available from: https://doi.org/10.1016/j.est.2023.109802.

[9] H. Wang, C. Zhou, Y. Wang, N. Li, J. Xiong, Phase change composite fiber membranes based on polyurethane/polyethylene glycol/silica with super-wetting and photothermal properties 77(December 2023), 2024.

[10] M. Jiang, X. Song, G. Ye, J. Xu, Preparation of PVA/paraffin thermal regulating fiber by in situ microencapsulation, Compos. Sci. Technol. 68 (10−11) (2008) 2231–2237.

[11] X.X. Zhang, X.C. Wang, X.M. Tao, K.L. Yick, Structures and properties of wet spun thermo-regulated polyacrylonitrile-vinylidene chloride fibers, Text. Res. J. 76 (5) (2006) 351–359.

[12] W. Li, Y.J. Ma, X.F. Tang, N. Jiang, R. Zhang, N. Han, et al., Composition and characterization of thermoregulated fiber containing acrylic-based copolymer microencapsulated phase-change materials (MicroPCMs), Ind. Eng. Chem. Res. 53 (13) (2014) 5413–5420.

[13] D. Luo, F. Wei, H. Shao, L. Xiang, J. Yang, Z. Cui, et al., Shape stabilization, thermal energy storage behavior and thermal conductivity enhancement of flexible paraffin/MWCNTs/PP hollow fiber membrane composite phase change materials, J. Mater. Sci. 53 (22) (2018) 15500–15513 [Internet]. Available from: https://doi.org/10.1007/s10853-018-2722-5.

[14] G. Li, G. Hong, D. Dong, W. Song, X. Zhang, Multiresponsive graphene-aerogel-directed phase-change smart fibers, Adv. Mater. 30 (30) (2018) 1–8.

[15] L. Xiang, D. Luo, J. Yang, X. Sun, J. Jin, S. Qin, Construction and Design of Paraffin/ PVDF hollow Fiber linear-phase change energy storage materials, Energy & Fuels 33 (11) (2019 Nov 21) 11584–11591 [Internet]. [cited 2022 Oct 10]. Available from: https://doi.org/10.1021/acs.energyfuels.9b02852.

[16] Y. Yan, W. Li, R. Zhu, C. Lin, R. Hufenus, Flexible Phase Change Material Fiber: A Simple Route to Thermal Energy Control Textiles, Mater 14 (2021) 401 [Internet]. 2021 Jan 15 [cited 2022 Oct 10];14(2):401. Available from: https://www mdpi.com/1996-1944/14/2/401/htm.

[17] W. Hu, X. Yu, Encapsulation of bio-based PCM with coaxial electrospun ultrafine fibers, RSC Adv. [Internet] 2 (13) (2012 Jun 13) 5580–5584 [cited 2022 Oct 10]. Available from: https://pubs.rsc.org/en/content/articlehtml/2012/ra/c2ra20532g.

[18] S.I. Golestaneh, A. Mosallanejad, G. Karimi, M. Khorram, M. Khashi, Fabrication and characterization of phase change material composite fibers with wide phase-transition temperature range by co-electrospinning method, Appl. Energy 182 (2016 Nov 15) 409–417.

[19] A. Babapoor, G. Karimi, S.I. Golestaneh, M.A. Mezjin, Coaxial electro-spun PEG/PA6 composite fibers: fabrication and characterization, Appl. Therm. Eng. 118 (2017 May 25) 398–407.

[20] M.E. Darzi, S.I. Golestaneh, M. Kamali, G. Karimi, Thermal and electrical performance analysis of co-electrospun-electrosprayed PCM nanofiber composites in the presence of graphene and carbon fiber powder, Renew. Energy 135 (2019 May 1) 719–728.

[21] C. Chen, L. Wang, Y. Huang, A novel shape-stabilized PCM: electrospun ultrafine fibers based on lauric acid/polyethylene terephthalate composite, Mater. Lett. 62 (20) (2008 Jul 31) 3515–3517.

[22] E. Zdraveva, J. Fang, B. Mijovic, T. Lin, Electrospun poly(vinyl alcohol)/phase change material fibers: morphology, heat properties, and stability, Ind. Eng. Chem. Res. [Internet] 54 (35) (2015 Sep 9) 8706–8712 [cited 2022 Oct 10]. Available from: https://doi.org/10.1021/acs.iecr.5b01822.

[23] M. Duran, A. Serrano, A. Nikulin, J.L. Dauvergne, L. Derzsi, E. Palomo del Barrio, Micro- capsule production by droplet microfluidics: A review from the material science approach, Mater. Des. 223 (2022) 111230 [Internet]. Available from: https://doi.org/10.1016/j.matdes.2022.111230.

[24] S. Lone, H.M. Lee, G.M. Kim, W.G. Koh, I.W. Cheong, Facile and highly efficient micro- encapsulation of a phase change material using tubular microfluidics, Colloids Surfaces A Physicochem Eng Asp. 422 (2013) 61–67.

[25] Z. Fu, L. Su, J. Li, R. Yang, Z. Zhang, M. Liu, et al., Elastic silicone encapsulation of n-hexadecyl bromide by microfluidic approach as novel microencapsulated phase change materials, Thermochim. Acta 590 (2014) 24–29.

[26] J. Li, L. Jia, Y. Chen, L. Li, S. Mo, J. Wang, et al., Microfluidic fabrication and thermal properties of microencapsulated n-heptadecane with hexanediol diacrylate shell for thermal energy storage, Appl. Therm. Eng. 162 (2019 Nov).

[27] X. Han, T. Kong, P. Zhu, L. Wang, Microfluidic encapsulation of phase-change materials for high thermal performance, Langmuir 36 (28) (2020 Jul) 8165–8173.

[28] T. Shi, P. Hu, J. Wang, Preparation of polyurea microcapsules containing phase change materials using microfluidics, ChemistrySelect 5 (7) (2020 Feb) 2342–2347.

[29] X. Zhang, R. Xie, W.X. Hu, Y. Faraj, Q. Zhao, X.X. Fan, et al., Microfluidic fabrication of core–sheath composite phase change microfibers with enhanced thermal conductive property, J. Mater. Sci. 53 (23) (2018 Dec 1) 15769–15783.

[30] M. Duran, A. Nikulin, A. Serrano, J.-L. Dauvergne, Y. Grosu, J. Labidi, et al., Jet-injection in situ production of PVDF/PCM composite fibers for thermal management, ACS Omega 8 (29) (2023 Jul 12) 26136–26146.

[31] H. Na, P. Chen, S.C. Wong, S. Hague, Q. Li, Fabrication of PVDF/PVA microtubules by coaxial electrospinning, Polymer (Guildf) 53 (13) (2012 Jun 7) 2736–2743.

[32] C.A. Schneider, W.S. Rasband, K.W. Eliceiri, NIH image to ImageJ: 25 years of image analysis, Nat. Methods 9 (7) (2012) 671–675 [Internet]. Available from: https://doi.org/10.1038/nmeth.2089.

[33] S.E. Gustafsson, Transient plane source techniques for thermal conductivity and thermal diffusivity measurements of solid materials, Rev. Sci. Instrum. 62 (3) (1991) 797–804.

[34] ISO 22007-2. ISO 22007-2: Plastics — Determination of thermal conductivity and thermal diffusivity — Part 2: Transient plane heat source (hot disc) method, Annu B ASTM Stand 2008 (2008) 17.

[35] J.T. Jung, J.F. Kim, H.H. Wang, E. di Nicolo, E. Drioli, Y.M. Lee, Understanding the non-solvent induced phase separation (NIPS) effect during the fabrication of microporous PVDF membranes via thermally induced phase separation (TIPS), J. Memb. Sci. 514 (2016) 250–263 [Internet]. Available from: https://doi.org/10.1016/j.memsci.2016.04.069.

[36] J. Lee, B. Park, J. Kim, Park S. Bin, Effect of PVP, lithium chloride, and glycerol additives on PVDF dual-layer hollow fiber membranes fabricated using simultaneous spinning of TIPS and NIPS, Macromol. Res. 23 (3) (2015) 291–299.

[37] P. Martins, J.S. Nunes, G. Hungerford, D. Miranda, A. Ferreira, V. Sencadas, et al., Local variation of the dielectric properties of poly(vinylidene fluoride) during the α- to β-phase transformation, Phys. Lett. A 373 (2) (2009 Jan 5) 177–180.

[38] J. Gomes, J. Serrado Nunes, V. Sencadas, S. Lanceros-Mendez, Influence of the β-phase content and degree of crystallinity on the piezo- and ferroelectric properties of poly (vinylidene fluoride), Smart Mater. Struct. 19 (6) (2010 Jun 1) 065010 [Internet]. Available from: https://doi.org/10.1088/0964-1726/19/6/065010.

[39] W. Huang, K. Edenzon, L. Fernandez, S. Razmpour, J. Woodburn, P. Cebe, Nano-composites of poly(vinylidene fluoride) with multiwalled carbon nanotubes, J. Appl. Polym. Sci. 115 (6) (2010 Mar 15) 3238–3248 [Internet]. Available from, https://doi.org/10.1002/app.31393.

[40] X. Cai, T. Lei, D. Sun, L. Lin, A critical analysis of the α{,} β and γ phases in poly-(vinylidene fluoride) using FTIR, RSC Adv. [Internet] 7 (25) (2017) 15382–15389. Available from: https://doi.org/10.1039/C7RA01267E.

[41] R. Gregorio Jr., M. Cestari, Effect of crystallization temperature on the crystalline phase content and morphology of poly(vinylidene fluoride), J. Polym. Sci. Part B Polym. Phys. [Internet] 32 (5) (1994) 859–870. Available from: https://doi.org/10.1002/polb.1994.090320509.

[42] D.A. Porter, T.V.T. Hoang, T.A. Berfield, Effects of in-situ poling and process parameters on fused filament fabrication printed PVDF sheet mechanical and electrical properties, Addit. Manuf. 13 (2017 Jan 1) 81–92.

[43] B. Mohammadi, A.A. Yousefi, S.M. Bellah, Effect of tensile strain rate and elongation on crystalline structure and piezoelectric properties of PVDF thin films, Polym. Test. 26 (1) (2007 Feb 1) 42–50.

[44] P.K. Mahato, A. Seal, S. Garain, S. Sen, Effect of fabrication technique on the crystalline phase and electrical properties of PVDF films, Mater. Sci. 33 (1) (2015) 157–162, https://doi.org/10.1515/msp-2015-0020.

[45] Tao M. Mi, F. Liu, Ma B. Rong, Xue L. Xin, Effect of solvent power on PVDF membrane polymorphism during phase inversion, Desalination 316 (2013 May 1) 137–145.

[46] Z. He, F. Rault, M. Lewandowski, E. Mohsenzadeh, F. Salaün, Electrospun PVDF Nanofibers for Piezoelectric Applications: A Review of the Influence of Electrospinning Parameters on the β Phase and Crystallinity Enhancement, Polymers (Basel) 13 (2) (2021) [Internet]. Available from: https://www.mdpi.com/2073-4360/13/2/174.

[47] S. Begum, H. Ullah, I. Ahmed, Y. Zhan, A. Kausar, M.A. Aleem, et al., Investigation of morphology, crystallinity, thermal stability, piezoelectricity and conductivity of PVDF nanocomposites reinforced with epoxy functionalized MWCNTs, Compos. Sci. Technol. [Internet] 211 (October 2020) (2021) 108841. Available from: https://doi.org/10.1016/j.comp-scitech.2021.108841.

[48] A. Mandal, A.K. Nandi, Physical properties of poly(vinylidene fluoride) composites with polymer functionalized multiwalled carbon nanotubes using nitrene chemistry, J. Mater. Chem. 21 (39) (2011) 15752–15763.

[49] E. Pramono, A.L. Simamora, C.L. Radiman, D. Wahyuningrum, Effects of PVDF concentration on the properties of PVDF membranes, IOP Conf Ser Earth Environ. Sci. 75 (1) (2017).

[50] J.E. Lee, Y.E. Shin, G.H. Lee, J. Kim, H. Ko, H.G. Chae, Polyvinylidene fluoride (PVDF)/ cellulose nanocrystal (CNC) nanocomposite fiber and triboelectric textile sensors, Compos Part B Eng [Internet] 223 (December 2020) (2021) 109098. Available from: https://doi.org/10.1016/j.compositesb.2021.109098.

[51] R. Atif, J. Khaliq, M. Combrinck, A.H. Hassanin, N. Shehata, E. Elnabawy, et al., Solution blow spinning of polyvinylidene fluoride based fibers for energy harvesting applica- tions: a review, Polymers (Basel) 12 (6) (2020) 1–29.

[52] B. Damdinov, Rheological properties of PVDF solutions, J. Sib. Fed. Univ. Math. Phys. (2021) 265–272.
[53] U. Domanska, D. Wyrzykowska-Stankiewicz, Enthalpies of fusion and solid-solid transition of even-numbered paraffins C22H46, C24H50, C26H54 and C28H58, Thermochim. Acta. [Internet] 179 (1991 Apr 19) 265–271 [cited 2019 Sep 12]. Available from: https://www.sciencedirect.com/science/article/abs/pii/004060319180356N.
[54] O.H. Wiener, Die theorie des mischkörpers für das feld der stationären strömung. 1. abhandlung: Die mittelwertsätze für kraft, polarisation und energie [Internet]. B. G. Teubner; 1912. (Abhandlungen der Mathematisch-physischen klasse der Königl. sächsischen gesellschaft der wissenschaften), Available from: https://books.google.es/books?id=i5UyHQAACAAJ.